

Review

Open Access



# Energy transfer process, luminescence optimizing and various applications of lanthanide complexes

Wei Fan, Huijuan Wang, Xuejian Huang, Tingchang Shi, Jing Du, Hai-Bing Xu\*

Collaborative Innovation Center for Advanced Organic Chemical Materials Co-constructed by the Province and Ministry, Ministry of Education Key Laboratory for the Synthesis and Application of Organic Functional Molecules, College of Chemistry and Chemical Engineering, Hubei University, Wuhan 430062, Hubei, China.

\***Correspondence to:** Prof. Hai-Bing Xu, Collaborative Innovation Center for Advanced Organic Chemical Materials Co-constructed by the Province and Ministry, Ministry of Education Key Laboratory for the Synthesis and Application of Organic Functional Molecules, College of Chemistry and Chemical Engineering, Hubei University, Youyi Avenue, No.368, Wuhan 430062, Hubei, China. E-mail: xhb@hubu.edu.cn

**How to cite this article:** Fan W, Wang H, Huang X, Shi T, Du J, Xu HB. Energy transfer process, luminescence optimizing and various applications of lanthanide complexes. *Chem Synth* 2024;4:12. <https://dx.doi.org/10.20517/cs.2023.35>

**Received:** 11 Jul 2023 **First Decision:** 22 Sep 2023 **Revised:** 28 Dec 2023 **Accepted:** 15 Jan 2024 **Published:** 29 Jan 2024

**Academic Editors:** Bao-Lian Su, Hai-Bing Xu, Da-Gang Yu **Copy Editor:** Dong-Li Li **Production Editor:** Dong-Li Li

## Abstract

Modulating the spectroscopic overlap between the emission bands of donors and the absorption spectra of acceptors by various simulations, it is possible to systematically investigate the emission behaviors of lanthanide complexes under different conditions. To establish the relationships between emission behaviors and various external simulations, it is necessary to study the energy transfer rate and efficiency between the donor and acceptor under different conditions to clarify the luminescent mechanism of the complexes, providing a theoretical basis for high-performance smart materials. This review focuses on the recent progress of luminescence performance of lanthanide complexes, including energy transfer mechanisms, emission color modulation, the strategies for optimizing lanthanide luminescence, and finally, various applications based on luminescence performance of lanthanide complexes and lanthanide metal-organic frameworks.

**Keywords:** Lanthanide complexes, downshifting luminescence, upconversion luminescence, molecular motor, pH-responsive delivery, dual-modal imaging

## INTRODUCTION

The special optical, especially their characteristic sharp bands of downshifting luminescence (DL) and upconversion luminescence (UCL) of lanthanide complexes enable them wildly in numerous applications



© The Author(s) 2024. **Open Access** This article is licensed under a Creative Commons Attribution 4.0 International License (<https://creativecommons.org/licenses/by/4.0/>), which permits unrestricted use, sharing, adaptation, distribution and reproduction in any medium or format, for any purpose, even commercially, as long as you give appropriate credit to the original author(s) and the source, provide a link to the Creative Commons license, and indicate if changes were made.



and technologies<sup>[1]</sup>, for instances, multiple signal detections<sup>[2]</sup>, barcoded materials<sup>[3]</sup>, and bioimaging nano-probes<sup>[4]</sup>, and even multiple detections for luminescent imaging in bioprobes<sup>[5]</sup>, among others. Due to the Laporte rule, the excited energy of lanthanide ions (Ln<sup>III</sup>) is usually efficiently populated by their surroundings<sup>[6]</sup>, which transfer their absorbed energies into the excited states of lanthanide, lighting up typical Ln<sup>III</sup>-based luminescence<sup>[7]</sup>. Since the triplet excited energies of photosensitizers are susceptible to external stimuli, their excited energies dependent on external simulations variously overlap the absorption spectra of given Ln<sup>III</sup>. Benefiting from inert transitions of Ln<sup>III</sup> for shielding effect, the changes of luminescence performance of lanthanide complexes smartly reflect their peripheral environment. Thus, the principles of the design of smart lanthanide complexes depend on modulation of energy levels between photosensitizers by different means and Ln<sup>III</sup>, adjusting their energy transfer rates and efficiencies<sup>[8]</sup>.

This review dominantly focuses on the recent progress of luminescence performance of lanthanide complexes mainly reported in our group. Three sections were involved. One was the energy transfer mechanism, including intermolecular sensitization for DL and UCL. Another was modulation of emission color and strategies for optimizing lanthanide luminescence through vibrational modes and rotational and trigger modes. The last one included various applications, such as water-soluble and luminescent imaging of lanthanide functionalized molecular motors and pH-responsive delivery and dual-modal imaging of lanthanide metal-organic frameworks (Ln-MOFs). Also, we point out the confusion on UCL of lanthanide complexes in solution, especially for bio-imaging and therapy.

## INTERMOLECULAR OR INTRAMOLECULAR ENERGY

Through the antenna effect, efficient lanthanide luminescence is usually achieved by employing aromatic ligands or d-block chromophores adjacent to Ln<sup>III</sup> as sensitizers<sup>[9]</sup>. That is, population of the typical lanthanide luminescence is operative through intramolecular or intermolecular energy transfer from adjacent sensitizers. The former approach requires significant synthetic efforts to functionalize bridging connectors directly bounding to the lanthanide emitters by chelation or linking<sup>[10]</sup>, promoting superposition of the emission bands of the sensitizers and the absorption spectra of the emitter mainly by the Dexter mechanism, also including the Förster mechanism. Alternatively, to avoid complicated and tedious synthesis, intermolecular sensitization is simply operative by closing both of them through van der Waals/Coulomb forces, such as ion-associated sensitization within ionic pair, noncovalent ligand-to-ligand interactions, and even cation- $\pi$  interactions in a bioinspired scaffold. As intermolecular energy transfer is operative through-space, besides the absorption coefficient of sensitizers, the energy transfer efficiency ( $h$ ) through the Förster mechanism strongly depends on their spatial separations; thus, high concentrations closing them to promote  $h$  are needed [Table 1].

### Ion-associated sensitization for DL

It is desirable to employ transition metal luminophores as the sensitizers, which easily red-shift the ligand-to-metal charge transfer (<sup>3</sup>LMCT) or metal-to-ligand charge transfer (<sup>3</sup>MLCT) absorption bands into a visible region<sup>[10]</sup>, facilitating efficient  $d \rightarrow f$  energy transfer to energize adjacent Ln<sup>III</sup><sup>[11]</sup>. Xu *et al.* reported the first example affording near-infrared (NIR) lanthanide luminescence by intermolecular  $d \rightarrow f$  sensitization across supramolecular interactions within the ionic  $d$ - $f$  heterometallic architecture of Ru-Er<sup>[12]</sup>.

In the crystal structure, every [Ru(bpy)<sub>2</sub>(dbim)]<sup>2+</sup> (2,2'-bipyridine, bpy; 2,2'-dibenzimidazole, dbim) was adjacent to three [Er(hfac)<sub>3</sub>]<sup>-</sup> moieties by C-H...F interactions with the shortest Ru<sup>II</sup>...Er<sup>III</sup> distance ca. 8.71 Å [Figure 1], within the Förster sphere for energy transfer. They had demonstrated NIR Er<sup>III</sup>-based luminescence was indeed lightened through an ion-associated sensitizer of Ru-subunit when irradiated

**Table 1. Comparison between intermolecular and intramolecular energy transfer in discrete lanthanide complexes**

	Intermolecular energy transfer	Intramolecular energy transfer
Synthesis	Simple	Complicate
Interaction	Van der Waals/Coulomb forces	Chelation/linking
Energy transfer efficiency	Low	High
Concentration	High	Low

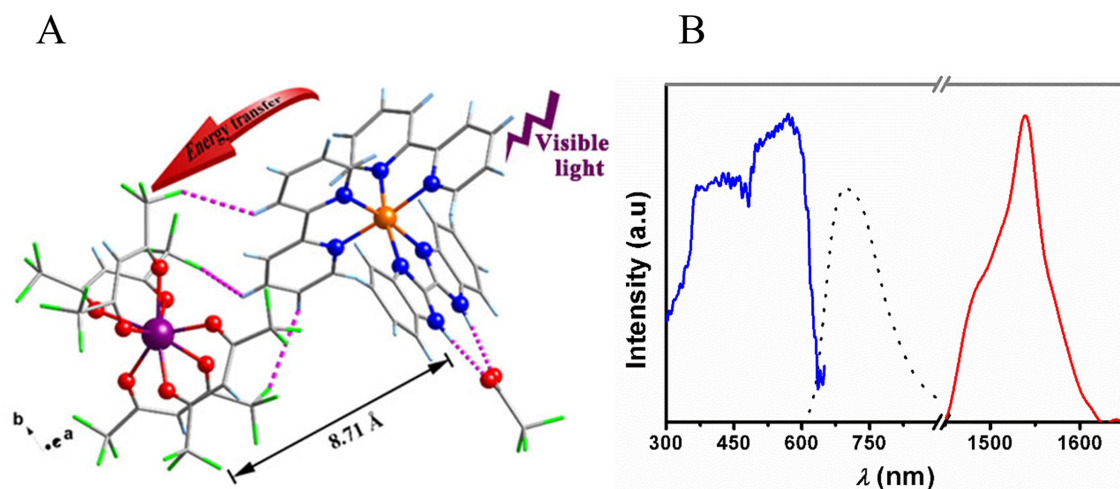


**Figure 1.** (A) Interactions among [Ru(bpy)<sub>2</sub>(dbim)]<sup>2+</sup>/[Er(hfac)<sub>4</sub>]<sup>3-</sup>; (B) luminescence spectra of Ru-Er [ $\lambda_{\text{ex}} = 420$  nm, Er<sup>III</sup> (red); residual Ru<sup>II</sup> (black)] in solid state. This figure is used with permission from the Royal Society of Chemistry<sup>[12]</sup>.

within its <sup>3</sup>MLCT absorption band. However, the typical Er<sup>III</sup>-based luminescence could not be observed in solutions since a large number of solvent molecules dispersed the Ru<sup>II</sup>...Er<sup>III</sup> distances out of the effective diameter of the Förster energy transfer.

### Ion-associated sensitization for UCL

The upconversion (UC) of NIR to visible (vis) photons is attracted in the fields of display technology and energy conversion. Due to the pronounced nonradiative excited energy exhaustion of -XH (X = O, N, C) in organic ligands<sup>[13]</sup>, the UC processes are usually confined to solids and nanoparticles<sup>[14,15]</sup>. Considering surface quenching effect and reproducibility<sup>[16]</sup>, it is necessary to reduce the UC system to the molecular scale<sup>[17]</sup>. Although confronted with difficulties, the Ion-associated sensitization for UCL of discrete lanthanide-organic complexes in solution is fancy.

### Dye-to-Er intermolecular energy transfer for UCL

Besides DL by intermolecular energy transfer, Hyppänen *et al.* realized molecular photon UCL even through intermolecular dye-to-Er energy transfer in Er(tta)<sub>4</sub>(IR-806) (tta = 2-thenoyltrifluoroacetate, IR-806 = NIR-emitting cyanine dye) in anhydrous solution under ambient atmosphere [Figure 2]<sup>[18]</sup>. In this setup, the IR-806 dye showed an absorption band centered at 808 nm and emission spectra at 827 nm. Upon irradiation at 808 nm, dual luminescences at ca. 510-540 nm (<sup>2</sup>H<sub>11/2</sub> → <sup>4</sup>I<sub>15/2</sub>) and 540-565 nm (<sup>2</sup>S<sub>3/2</sub> → <sup>4</sup>I<sub>15/2</sub>) of Er<sup>III</sup> appeared in Er(tta)<sub>4</sub>(IR-806) rather than in Er(tta)<sub>4</sub>K or IR-806 dye. These facts suggested it was indeed by intermolecular energy transfer from IR-806 dye to Er<sup>3+</sup> that triggered UCL at 510-565 nm by 808 nm irradiation. Also, the UCL was second-order dependent on the density of excitation power (*P*), suggesting an intermolecular dye-sensitized energy transfer upconversion (ETU) mechanism.

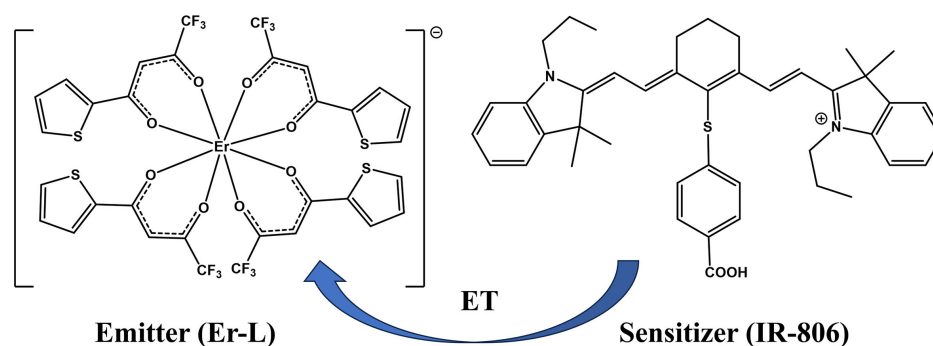


**Figure 2.** Chemical structure of ion pair of  $\text{Er}(\text{TTA})_4(\text{IR-806})$ . This figure is used with permission from the American Chemical Society<sup>[18]</sup>. ET: Energy transfer.

### Yb-to-rubrene collisional energy transfer for UCL

Although triplet-triplet annihilation (TTA) is considered as an efficient approach for UCL under low  $P$ <sup>[19]</sup>, it is still confronted with fundamental limitations by current strategies for NIR-vis UC. Howard and Turshatov employed Yb sensitizers to generate TTA-UCL by intermolecular energy transfer to the triplet state of the rubrene annihilator through  $S_0 \rightarrow T_1$  sensitization<sup>[20]</sup>. Due to the absence of covalent or supramolecular interactions between Yb subunits and rubrene, they proposed that the UC process was operative through collisional energy transfer from a  $\text{Yb}(\beta\text{-diketonate})_3$  to rubrene, emitting yellow UCL at 559 nm under laser irradiation at 980 nm [Figure 3].

### Cr-to-Yb energy transfer for NIR UCL

According to energy levels between  $\text{Cr}^{3+} (^2E/^2T_1)$ <sup>[21]</sup> and  $\text{Yb}^{3+} (^2F_{5/2})$ ,  $\text{Cr}^{3+}/\text{Yb}^{3+}$ -architectures could operate *via* cooperatively sensitized upconversion (CSU), in which two  $\text{Yb}^{3+} (^2F_{5/2})$  cooperatively transfer their excited energies into an excited state  $^4T_2/^4T_1$  of  $\text{Cr}^{3+}$ , populating UCL at 755 nm, which corresponds to the transitions of  $\text{Cr}^{\text{III}}$  from  $^2E$  state to the ground state ( $^4A_2$ ) [Figure 4]. However, due to possible  $^2E (\text{Cr}^{3+}) \rightarrow ^2F_{5/2} (\text{Yb}^{3+})$  transitions in  $\text{Cr}^{3+}/\text{Yb}^{3+}$ -architectures, it seems unsuitable for UC processes<sup>[22]</sup>.

To efficiently prevent downshifting energy transfer from  $^2E (\text{Cr}^{3+})$  to  $^2F_{5/2} (\text{Yb}^{3+})$ , Wang *et al.* constructed  $[\text{Cr}^{3+}][\text{Yb}^{3+}]$  ion pairs (named Cr-Yb) using  $[\text{Yb}(\text{dpa})_3]^{3-}$  (2,6-pyridine-dicarboxylate, dpa) as sensitizers and octahedral  $[\text{Cr}(\text{ddpd})_2]^{3+}$  ( $N,N'$ -dimethyl- $N,N'$ -dipyridine-2-ylpyridine-2,6-diamine, ddpd) as an activator for UCL, by Förster mechanism through spatial dispersion of metal centers. In the crystal structure, every  $\text{Cr}^{3+}$  activator was encompassed with five  $\text{Yb}^{3+}$  sensitizers within the nearest distances ( $8.75 \text{ \AA} < r_{\text{Cr-Yb}} < 9.07 \text{ \AA}$ ), falling the diameter of Förster energy transfer. Upon excitation at 435 nm into the  $^4A_2 \rightarrow ^4T_2$  band of  $[\text{Cr}(\text{ddpd})_2]^{3+}$ <sup>[23]</sup>, not only the expected  $\text{Cr}^{\text{III}}$ -based phosphorescence around 780 nm but also the presence of a  $\text{Yb}^{3+}$  luminescence at around 1,000 nm appeared. As  $\text{Na}_3[\text{Yb}(\text{dpa})_3] \cdot 6\text{H}_2\text{O}$  was non-emissive, these facts clearly indicated undesired  $\text{Cr} \rightarrow \text{Yb}$  energy transfer was still present in Cr-Yb. Unexpectedly, there was no UCL observed for Cr-Lu, but intensive UCL of the activator  $\text{Cr}^{3+}$  ( $\lambda_{\text{em}} = 780 \text{ nm}$ ) by excitation at 976 nm at  $P = 67 \text{ W} \cdot \text{cm}^{-2}$  in Cr-Yb appeared. Both excitation and UC emissions falling into the NIR region favor bioimaging.

### Yb-to-Eu intermolecular energy transfer for UCL

Recently, Sun *et al.* reported  $[\text{YbEu}]$  co-crystals constructed by discrete complexes  $\text{Yb}(\text{DBM})_3\text{Bpy}$  (sensitizer) and  $\text{Eu}(\text{DBM})_3\text{Bpy}$  (DBM = dibenzoylmethane) as an activator through noncovalent interactions, with the closest distance between  $\text{Yb}^{3+}$  and  $\text{Eu}^{3+}$  of 9.1 Å, for UCL through cooperative sensitization [Figure 5]<sup>[24]</sup>. Without resonance between the virtual state of  $\text{Yb}^{3+}$  and the excited states of  $\text{Eu}^{3+}$ ,

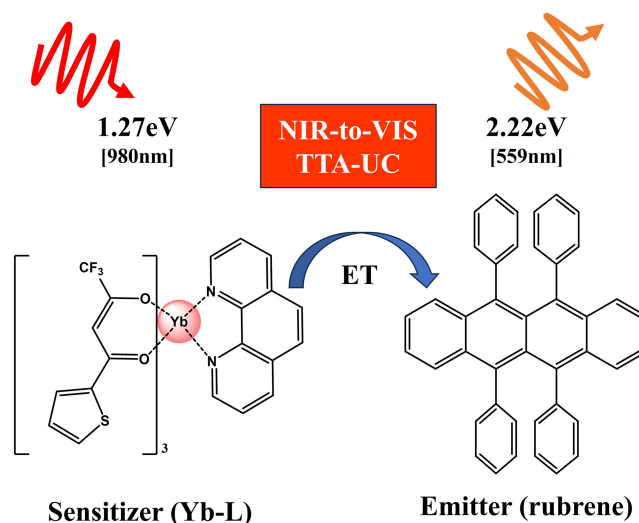


**Figure 3.** Scheme of TTA-UC within  $\text{Yb}(\beta\text{-diketonate})_3/\text{rubrene}$ . This figure is used with permission from the American Chemical Society<sup>[20]</sup>.

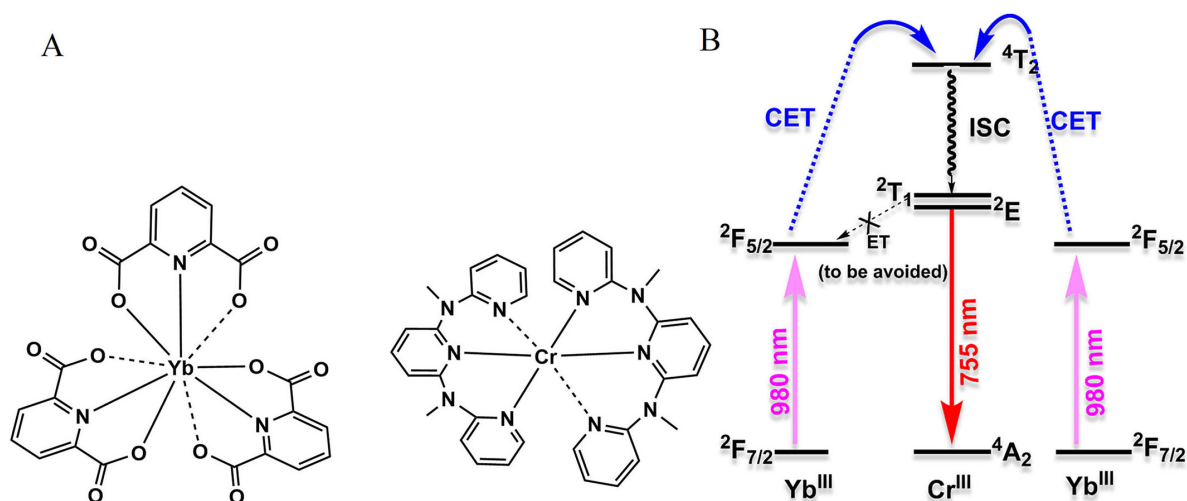


**Figure 4.** (A) Chemical structure of the **Cr-Yb**; (B) Schematic partial energy-level diagram of  $\text{Yb}^{3+}$  and  $\text{Cr}^{3+}$  relevant for CSU. This figure is used with permission from Wiley-VCH GmbH<sup>[21]</sup>. ISC: Intersystem crossing; CET: cooperative energy transfer; CSU: cooperatively sensitized upconversion.

they considered it was the simultaneous energy transfer from two  $\text{Yb}^{3+}$  ions that populated  $\text{Eu}^{3+}$  through cooperative sensitization UC. Moreover, the optimized  $\text{Yb}^{3+}:\text{Eu}^{3+}$  molar ratio of 1:1 for the most intense UCL with a quantum yield ( $\Phi_{\text{UC}}$ ) up to 0.67% at 2.1 W/cm<sup>2</sup>, it was considered that the rigid polyhedral structure formed by the ligands effectively protected both  $\text{Yb}^{3+}$  and  $\text{Eu}^{3+}$  from the quenching competitors, resulting in effective intermolecular energy transfer from  $\text{Yb}^{3+}$  to  $\text{Eu}^{3+}$ .

In brief, achieving both DL and UCL by intermolecular energy transfer not only provides a simpler way of avoiding tedious synthesis but also broadens the approaches for modulation of luminescence performance of lanthanide complexes. However, it is also confronted with low energy transfer efficiency from a donor to an acceptor, even operative in higher concentration solutions for UCL, which inevitably suffers from the

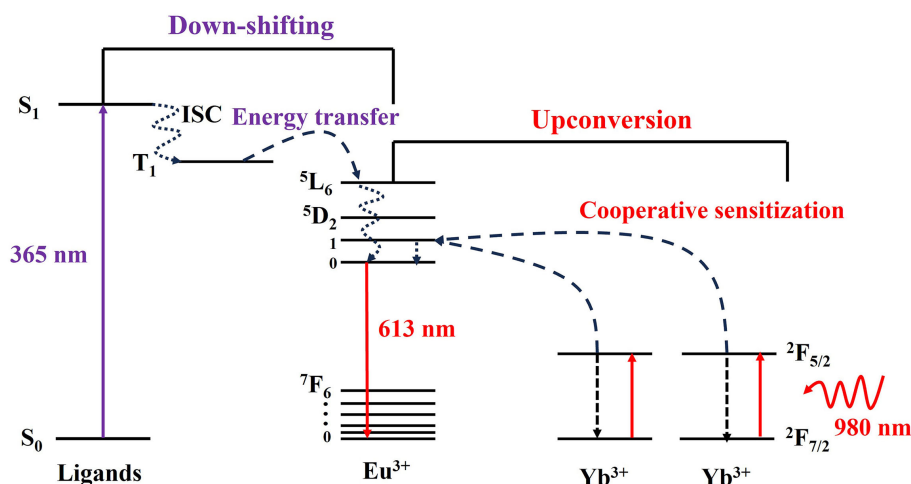


**Figure 5.** Mechanism of [YbEu] assembly for DL ( $\lambda_{\text{ex}} = 365$  nm) and UCL ( $\lambda_{\text{ex}} = 980$  nm). This figure is used with permission from Wiley-VCH GmbH<sup>[24]</sup>. ISC: Intersystem crossing; DL: downshifting luminescence; UCL: upconversion luminescence.

“aggregation-caused quenching” (ACQ) effect<sup>[25]</sup>. Moreover, regulating the excited photon transition pathway remains challenging.

## LUMINESCENCE REGULATION

### Emission color modulation

Traditionally, high extinction coefficient organic bridging ligands are usually employed as light harvesters to enhance lanthanide emission through the antennal effect. Thus, it is practicable to increase the rigidity of the bridging ligands for diverse structures<sup>[26]</sup> and also tune the emissive color by combining the residual emission of the sensitizers and the typical Ln<sup>III</sup>-based luminescence<sup>[27]</sup>. Xu *et al.* employed similar length but different conjugacy bridging ligands, bis(diphenylphosphine oxide) 1,4-butane (PBuPO<sub>2</sub>), bis(diphenylphosphine oxide)-1,4-benzene (PBePO<sub>2</sub>), and bis(diphenylphosphine oxide)-9,10-anthracene (PAnPO<sub>2</sub>) [Figure 6A] to react with Sm(hfac)<sub>3</sub>(H<sub>2</sub>O)<sub>2</sub> (hfac = hexafluoroacetylacetonato), affording one-dimensional ribbon {Sm(hfac)<sub>3</sub>(PBuPO<sub>2</sub>)<sub>3</sub>}<sub>∞</sub> (**Sm-PBuPO<sub>2</sub>**), two-dimensional layer {Sm<sub>2</sub>(hfac)<sub>5</sub>(PBePO<sub>2</sub>)<sub>6</sub>}<sub>∞</sub> (**Sm-PBePO<sub>2</sub>**), and zero-dimensional cyclic {Sm(hfac)<sub>3</sub>(PAnPO<sub>2</sub>)<sub>2</sub>}<sub>2</sub> (**Sm-PAnPO<sub>2</sub>**), respectively [Figure 6B]<sup>[28]</sup>. The configuration of the Sm<sup>III</sup>-based subunits changed from *trans*- in **Sm-PBuPO<sub>2</sub>** and **Sm-PBePO<sub>2</sub>** to *cis*- in **Sm-PAnPO<sub>2</sub>**. Additionally, the driving force of  $\pi \cdots \pi$  stacking interactions transferred from the intermolecular patterns between benzene rings in **Sm-PBuPO<sub>2</sub>** to the intramolecular one between anthracenyl rings in **Sm-PAnPO<sub>2</sub>**.

Interestingly, it is not only to control the structural dimensionality but also to regulate the emissive color of the complexes by increasing the conjugation of the bridging ligands. Due to the intermolecular  $\pi \cdots \pi$  stacking interactions between sensitizers, their emission bands gradually red-shift to cover the fixed Sm<sup>III</sup>-based ones, producing red (CIE = 0.72, 0.28), white (0.36, 0.35), and green color emissions (0.31, 0.68) for **Sm-PBuPO<sub>2</sub>**, **Sm-PBePO<sub>2</sub>**, and **Sm-PAnPO<sub>2</sub>**, respectively [Figure 6C]. This strategy provided a practicable way to regulate the structure performance of lanthanide luminescent materials [Figure 6D] and also afforded a feasible method to optimize lanthanide emission through modulating the spectroscopic overlap between the emission bands of the sensitizers and the absorptions of Ln<sup>III</sup> through various simulations.

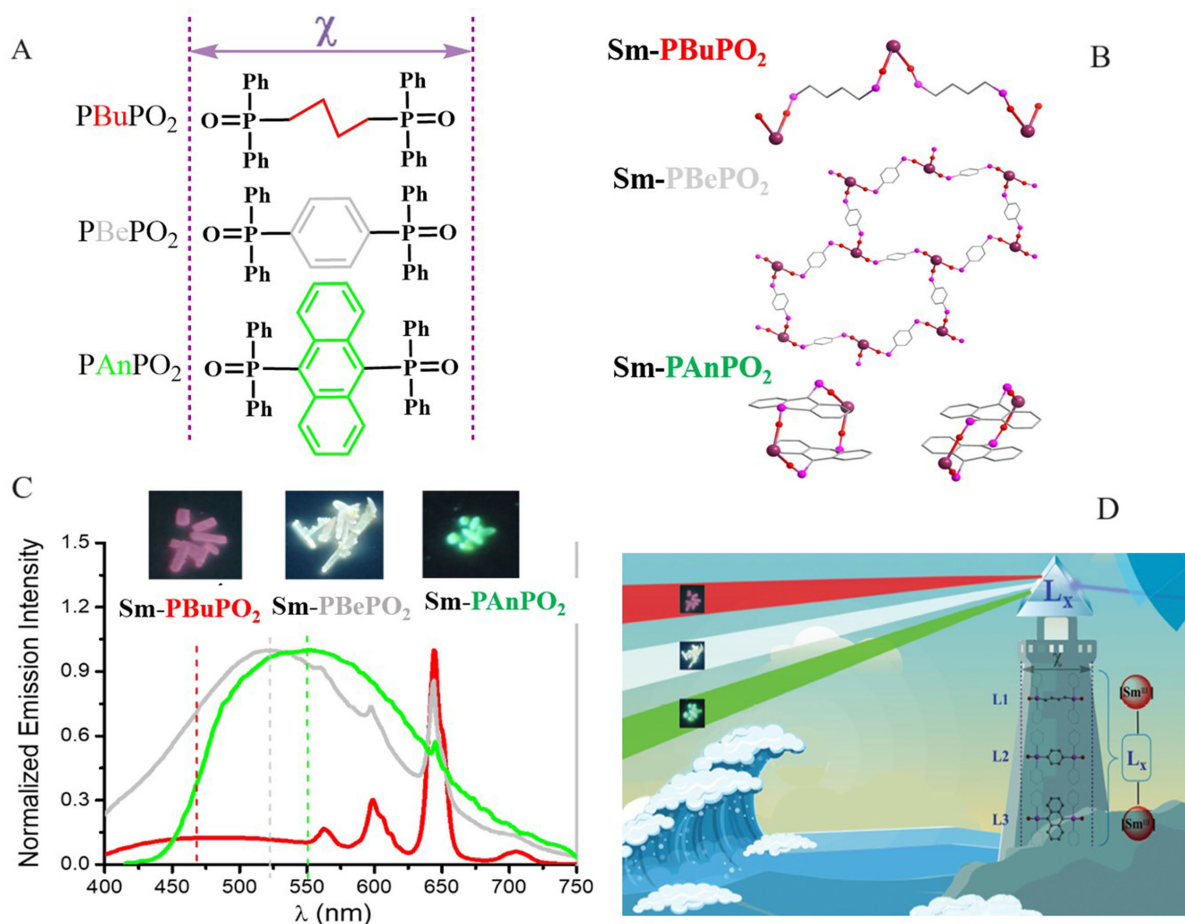


**Figure 6.** (A) Similar lengths but different levels of conjugacy of bridging ligands; (B) crystal structures of lanthanide complexes; (C) their emissions and corresponding colors depending on the bridging ligand in solid state; (D) spectroscopic function diagram of lanthanide complexes with similar lengths but different conjugated bridging ligands. This figure is used with permission from the Royal Society of Chemistry<sup>[28]</sup>.

Shifting emissive colors through UC at the molecular level holds more significant meaning compared to controlling emissive colors through down-conversion. Gálico *et al.* had successfully designed and synthesized a series of UC molecular clusters (MCAs) containing 15 Ln<sup>III</sup><sup>[29]</sup>. These clusters exhibited highly tunable compositions, particularly demonstrating excellent capabilities in adjusting emissive colors. For instance, {Er<sub>2</sub>Yb<sub>10</sub>}, {Y<sub>10</sub>Er<sub>1</sub>Yb<sub>4</sub>}, and {Er<sub>10</sub>Yb<sub>5</sub>} MCAs showed significant changes in emissive colors at different laser powers. At low laser power, the emitted light tended toward red, while with increasing power, it shifted toward green. This outstanding tunability in emissive colors was attributed to the molecular structure of MCAs. This structure not only increased the probability of energy transfer from Yb<sup>III</sup> to Er<sup>III</sup> but also enhanced the intensity of upconverted emissions, achieving an extremely high UC quantum yield (UCQY) of up to 10<sup>-3</sup>%.

## STRATEGY ON OPTIMIZING LANTHANIDE LUMINESCENCE

### Vibrational mode - walkable dual emissions

Regarding a molecule containing two types of luminophores, one is stationary, such as the lanthanide subunits, which is not sensitive to external stimulations. The other is a walker (conjugate aromatic ligands), and its emission behavior is susceptible to the outside environment. If the two chromophores are constructed into a square structure, the parallel walkers would readily experience  $\pi \cdots \pi$  stacking interactions,

enabling the emission spectra of the walker back and forth compared to those of the stationary. Xu *et al.* provided a cyclic structure of  $\{\text{PAnPO}_2\text{Eu}(\text{hfac})_3\}_2$  ( $\text{PAnPO}_2 = 9,10\text{-bis}(\text{diphenylphosphino})\text{anthracenedioxide}$ )<sup>[30]</sup>, in which the two coplanar anthracenes within 3.4 Å suffered from strong  $\pi\cdots\pi$  stacking interactions [Figure 7A]. Since such configuration possessed shorter distances between the two walkers in the aggregated state by  $\pi\cdots\pi$  stacking interactions than in the isolated state, the central emissive bands of  $\text{PAnPO}_2$  (the walker) red-shifted to close the  $\text{Eu}^{\text{III}}$ -based luminescence (the stationary) by increasing the concentrations [Figure 7B] or decreasing the measurement temperature [Figure 7C]. In turn, reversely diluting the solution concentrations, the emission bands of the walker leave that of the stationary stepwise. Further, using  $\text{Tb}^{\text{III}}$  instead of  $\text{Eu}^{\text{III}}$ , the  $\text{PAnPO}_2$ -based emissions red-shifted to cross the fixed  $\text{Tb}^{\text{III}}$ -based emissions rather than shield almost the  $\text{Eu}^{\text{III}}$  ones [Figure 7D]. Such non-destructive physical cycles enable these phenomena to be completely reversible and reliable. The walker shows bathochromic and hypsochromic behavior dependent on temperature and concentration, while the stator remains static throughout; the former can cross and leave the latter, depending on experimental environments. Thus, by precisely controlling the separations of adjacent walkers, the cyclic dimeric lanthanide would be promising in information gateways, providing a simple way to spread the information from one to another.

## ROTATIONAL MODE

### AIPE-activity of discrete NIR lanthanide architectures

Considering NIR materials for powders or thin films, it is necessary to broaden “aggregation-induced phosphorescence enhancement” (AIPE) family from transition metals to discrete NIR lanthanide compounds. As the excited state of organometallic luminogens and “aggregation-induced emission” (AIE) ligands are sensitive to external stimuli, it is theoretically challenged to afford the AIPE activity of metallic compounds through energy transfer<sup>[31]</sup>, although the AIPE on organic compounds has been reported for decades<sup>[32]</sup>. As far as lanthanide complexes are concerned, the shielding effect and the inner f-f electronic transitions enable their excited energies to be unsusceptible to the outside environment; the excited energies of ligands induced by aggregation could efficiently energize the lanthanide(III)-subunit, possibly affording AIPE-active lanthanide complexes.

Ideal sensitizers suitable for sensitizing NIR  $\text{Ln}^{\text{III}}$ -based luminescence have been demonstrated to mainly possess three combining features, including matched energy to the given NIR lanthanide ion, effectively reducing nonradiative dissipation, and low-energy shifting the excitation window [Figure 8]<sup>[33]</sup>. Herein, we afforded two NIR lanthanide complexes by employing AIE-active tetraphenylethylene (TPE) derivatives as sensitizers<sup>[34]</sup>; the crystal structure shows that the  $\text{Nd}^{\text{III}}$  chelates two ligands to furnish a ten-coordinate environment, leading to formation of  $\text{Nd}(\text{TPE}_2\text{-BPY})_2$  and  $\text{Nd}(\text{TPE-BPY})_2$ . The corresponding signals of Electrospray ion mass spectra (ESI-MS) under positive patterns confirmed their stabilities in solutions. Both  $\text{TPE}_2\text{-BPY}$  and  $\text{TPE-BPY}$  had matched energy to  $\text{Nd}^{\text{III}}$ , effectively preventing nonradiative processes by aggregation, even red-shifting the excitation wavelength through twisted intramolecular charge transfer. Moreover, the excited energies of the AIE-active sensitizers were significantly enhanced by structural rigidification, which energized the excited state of inert  $\text{Nd}^{\text{III}}$  through the antenna effect.

Since  $\text{TPE}_2\text{-BPY}$  was equipped with more TPE subunits than  $\text{TPE-BPY}$ , the luminescence enhancement in 90% *n*-hexane for the former (18 times) was more obvious than that of the latter (11 times) respect to those in no *n*-hexane, suggesting the AIE-activity of  $\text{TPE}_2\text{-BPY}$  was superior to that of  $\text{TPE-BPY}$ . Consequently,  $\eta_{\text{L}\rightarrow\text{Nd}}$  of  $\text{Nd}(\text{TPE}_2\text{-BPY})_2$  were superior to those of  $\text{Nd}(\text{TPE-BPY})_2$ . Additionally, the intensity amplification in 95% *n*-hexane of  $\text{Nd}(\text{TPE}_2\text{-BPY})_2$  (about 15 times) was more than that of  $\text{Nd}(\text{TPE-BPY})_2$  (1.8 times) with respect to that without *n*-hexane. It was reasonable to draw the conclusion that the  $\eta_{\text{L}\rightarrow\text{Nd}}$  dependent on the



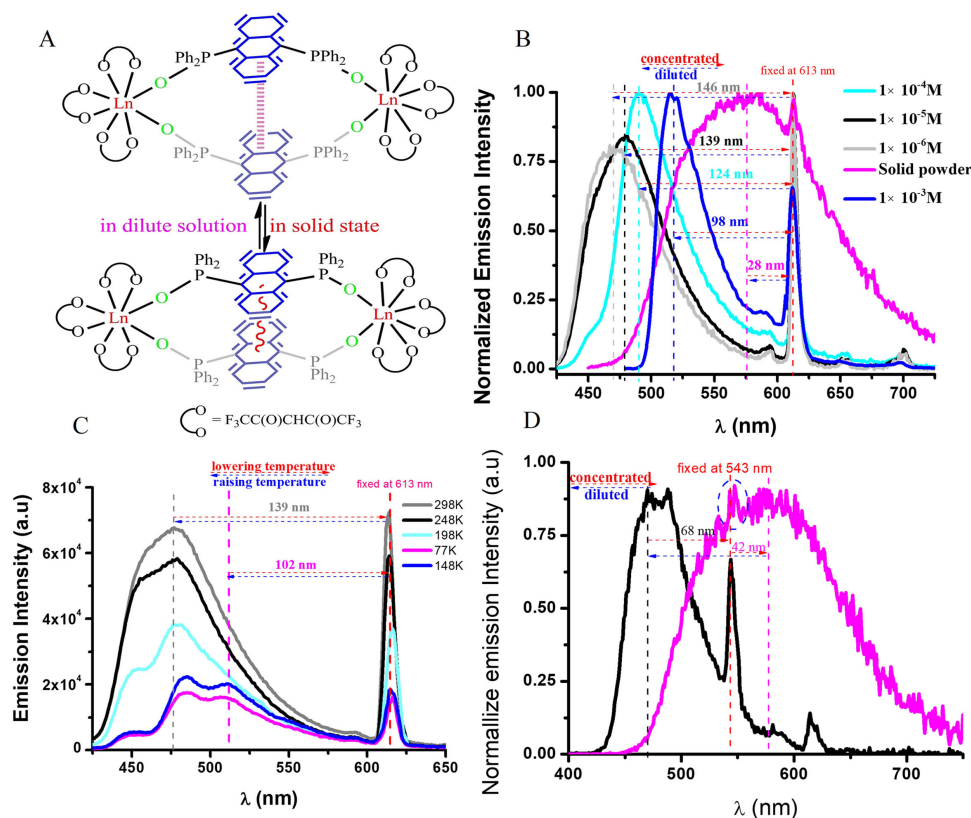


**Figure 7.** (A) Ring structures of  $\{PAnPO_2Eu(hfac)_3\}_2$  with vibrational modes; (B) normalized concentration-dependent luminescence ( $\lambda_{\text{ex}} = 350 \text{ nm}$ ); (C) normalized temperature-dependent emission ( $\lambda_{\text{ex}} = 350 \text{ nm}$ ) in  $\text{CH}_2\text{Cl}_2$  ( $1.5 \times 10^{-5} \text{ M}$ ); (D) normalized emission spectra of  $\{PAnPO_2Tb(hfac)_3\}_2$  ( $\lambda_{\text{ex}} = 330 \text{ nm}$ ) in  $\text{CH}_2\text{Cl}_2$  ( $1.5 \times 10^{-5} \text{ M}$ , black) and solid state (red) under room temperature. This figure is used with permission from Springer Nature<sup>[30]</sup>.

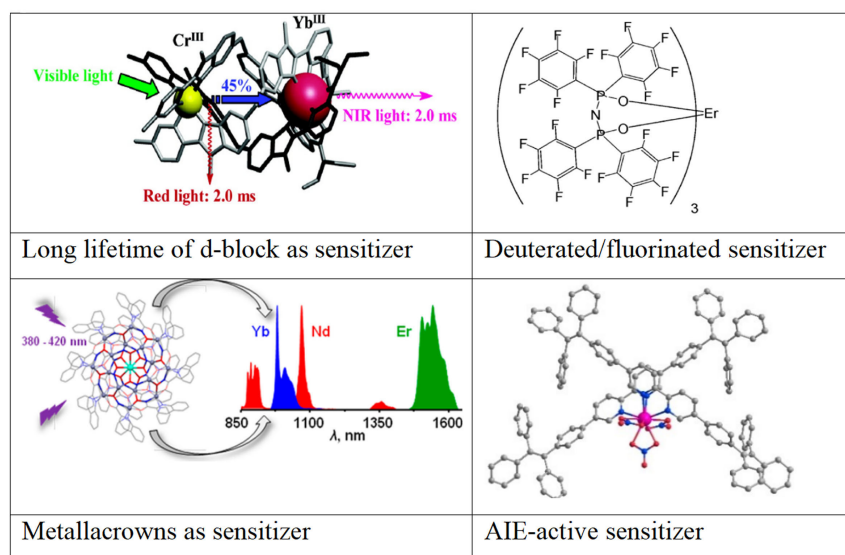


**Figure 8.** Strategy on optimizing NIR lanthanide luminescence performance. This figure is used with permission from the American Chemical Society<sup>[33]</sup>. AIE: Aggregation-induced emission; NIR: near-infrared.

number of TPE in sensitizers by structural rigidification, induces the crystal of  $\text{Nd}(\text{TPE}_2\text{-BPY})_2$  with one of the longest lifetimes (9.69  $\mu\text{s}$ ) among  $\text{Nd}^{\text{III}}$ -based complexes containing C–H bonds.

### Switchable sensitizers stepwise activated to lighten $\text{Ln}^{\text{III}}$ -based emissions

Ideal bioprobes are considered to have consistent signals with high sensitivity and resolution in any concentrations so that they could always be captured in complicated bioassay systems. However, it is hard to accomplish this aim for the common ACQ effect, hampering the detection of single luminescent molecules in high concentration solution<sup>[35]</sup>. Herein, the lanthanide complex  $[\text{TPE-TPY-Eu}(\text{hfac})_3]$  was reported to be equipped with switchable sensitizers [Figure 9A]. One was a “bladed” structure, TPE-TPY (4'-(4-(1,2,2-triphenylvinyl)phenyl)-2,2':6',2''-terpyridine) with AIE-activity, while the other was ACQ-active planar luminogenic hfac-, stepwise activating for consistent lanthanide emission triggered by variable concentrations [Figure 9B]<sup>[36]</sup>.

The excitation spectra of  $[\text{TPE-TPY-Eu}(\text{hfac})_3]$  ( $10^{-5}$  M) only resembled those of  $\text{Eu}(\text{hfac})_3 \cdot 2\text{H}_2\text{O}$ , not  $[\text{TPY-Eu}(\text{NO}_3)_3]$ , suggesting it was the main hfac- instead of TPY transferring the excited energy into the  $\text{Eu}^{3+}$  with  $\eta = 42.5\%$  in very dilute solutions ( $\leq 10^{-5}$  M). Additionally, the much lower emission intensity ( $\lambda_{\text{ex}} = 306$  nm) of  $[\text{TPE-TPY-Eu}(\text{NO}_3)_3]$  than that of  $[\text{TPY-Eu}(\text{NO}_3)_3]$  indicated it was the intramolecular rotations of TPE that consumed the excited energies of TPY, markedly reducing  $\eta_{\text{TPY} \rightarrow \text{Eu}}$ . All these facts confirmed it was the hfac- that sensitized the  $\text{Eu}^{\text{III}}$ -based emission at low concentrations.

As shown in Figure 9C, the maximal excitation wavelengths red-shifted to 426 nm from 310 nm by increasing the concentrations, suggesting different sensitizers in variable concentrations were stepwise activated to lighten lanthanide emission. Thus, different types (AIE and ACQ effects) of sensitizers were stepwise activated to energize  $\text{Eu}^{\text{III}}$ -based emissions. Also, the excitation wavelength extended from ca. 310 to 426 nm, and  $\Phi_{\text{em}}$  dropped from 3.8% to 0.16%, then up to 0.95% by increasing the concentrations [Figure 9D]. Moreover, a good linear relationship between  $I_{\text{ex}}$  vs.  $\{\lg(M)\}$  indicated that the concentration of  $[\text{TPE-TPY-Eu}(\text{hfac})_3]$  could be monitored digitally by  $I_{\text{ex}}$ , realizing consistent  $\text{Eu}^{\text{III}}$ -based emission within large-scale concentrations by switching the ACQ/AIE-active sensitizers, suitable in complicated bioassay systems.

### Trigger mode

Excluding statistical crystallization<sup>[37]</sup>, the control of the synthesis of heterometallic complexes containing more than two different  $\text{Ln}^{\text{III}}$  is confusing due to similar ionic radius and coordination preferences<sup>[38]</sup>. Making use of versatile ligating  $\mu_{2,3}$ -fashion of unsubstituted Hq (8-hydroxyquinoline),  $\{\text{Ln}_2(\text{hfac})\}_2[\mu_3\text{-OH}]_2$   $[\text{Ln}^*\text{q}(\text{hfac})_2]$  ( $\text{Ln}, \text{Ln}^* = \text{Er}, \text{Gd}, \text{Yb}$ , named  $[\text{Ln}]_2[\text{Ln}^*]_2$ ) with two types of lanthanide atoms were constructed [Figure 10A]<sup>[39]</sup>. Since the nonradiative O–H vibration from the direct linkage of  $\mu_3\text{-OH}^-$  to the  $\text{Ln}^{\text{III}}$  severely quenched the  $\text{Ln}^{\text{III}}$ -based luminescence, the introduction of 2 equivalents of fluoride to generate strong O–H...F interactions successfully prevented the vibrational nonradiative processes, inducing two-fold intensity enhancement of  $\text{Yb}^{\text{III}}$ -based luminescence, rather than the hoped-for UCL signals of  $[\text{Yb}]_2[\text{Er}]_2$  [Figure 10B].

Till now, both homonuclear erbium and discrete heteronuclear lanthanide architectures<sup>[40]</sup> exhibit weak molecular UCL with a low quantum yield ( $\Phi_{\text{UC}} < 0.1\%$ ), even under extreme conditions<sup>[41]</sup>. It has been demonstrated that UC processes in discrete heteronuclear lanthanide compounds through mixed mechanisms may afford highly intensive UCL in an aqueous solution<sup>[42,43]</sup>. Instead of traditional supramolecular chemical self-assembly for construction of heteronuclear lanthanide compositions<sup>[44]</sup>, Wang *et al.* employed tridentate  $\text{H}_2\text{hmq}$  (2-(hydroxymethyl)quinolin-8-ol) replacing bidentate Hq, affording  $\{[\text{Ln}_2\text{Ln}^*(\text{Hhmq})_3(\text{OAc})_3(\text{hfac})_2]^+ [\text{Ln}^*(\text{hfac})_3(\text{OAc})(\text{MeOH})]^- \}$  ( $\text{Ln}, \text{Ln}^* = \text{Er}, \text{Gd}, \text{Yb}$ )<sup>[45]</sup>. The presence of

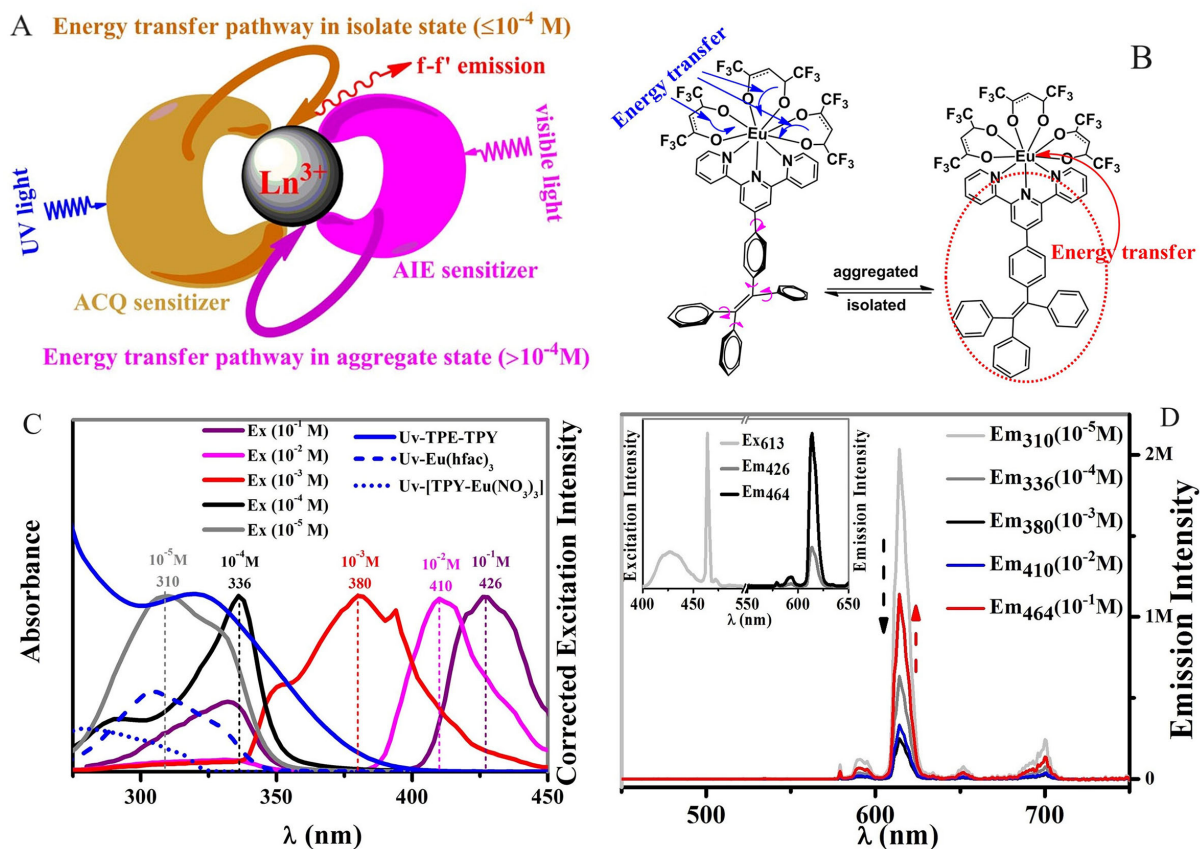


**Figure 9.** (A) Diagram of switchable TPE-TPY-Eu(hfac)<sub>3</sub>; (B) its emission spectra with different concentrations in CH<sub>2</sub>Cl<sub>2</sub>; (C) its excitation spectra ( $\lambda_{em} = 613$  nm) in different concentrations; (D) emission dependent on different concentrations in CH<sub>2</sub>Cl<sub>2</sub> at 298 K. This figure is used with permission from Springer Nature<sup>[36]</sup>. ACQ: Aggregation-caused quenching; AIE: aggregation-induced emission.

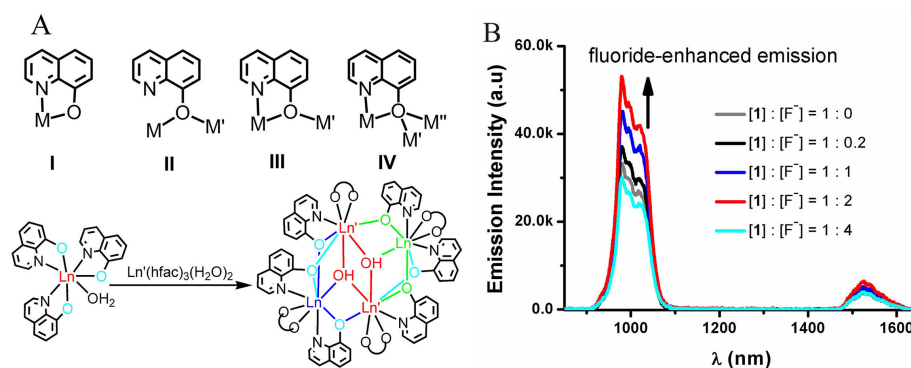


**Figure 10.** (A) Heteronuclear lanthanide complexes by metallic blocks orientational assembly; (B) their emission intensity depending on fluoride in CH<sub>2</sub>Cl<sub>2</sub>. This figure is used with permission from Springer Nature<sup>[39]</sup>.

corresponding signals of ESI-MS in positive models confirmed the consistency of solid-state/solution structures of the stable [Yb<sub>2</sub>Er]<sup>+</sup>/[Er<sub>2</sub>Yb]<sup>+</sup> core in solution [Figure 11A]. The  $\mu_2$ - and  $\mu_3$ -bridged two and three Ln atoms, with close Ln...Ln\* distances ( $< 3.7$  Å), favor energy transfer from sensitizer (S) to activator (A). Also, O-H...F interactions are employed to prevent nonradiative processes from the undehydrogenated hydroxymethyl group of Hhmq<sup>[-46]</sup>.

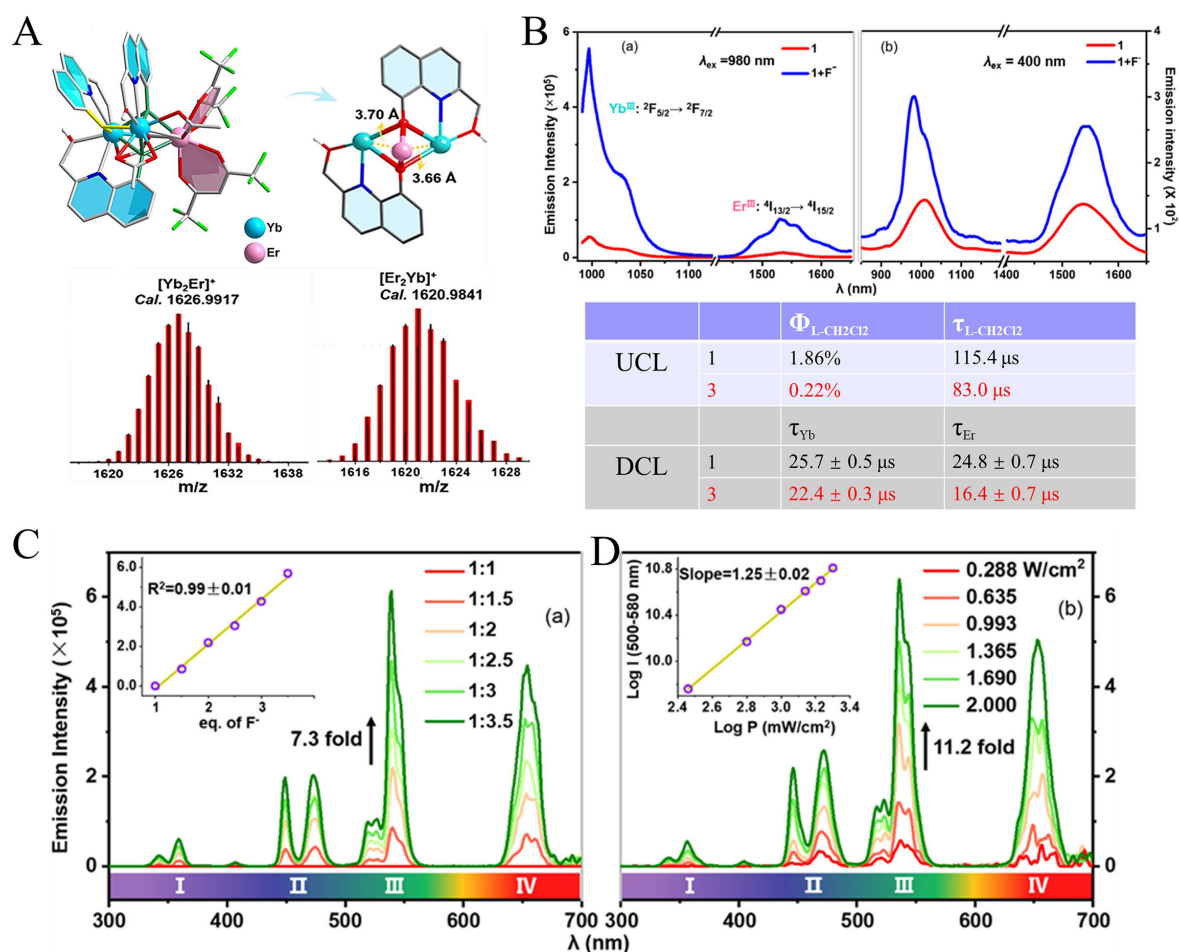
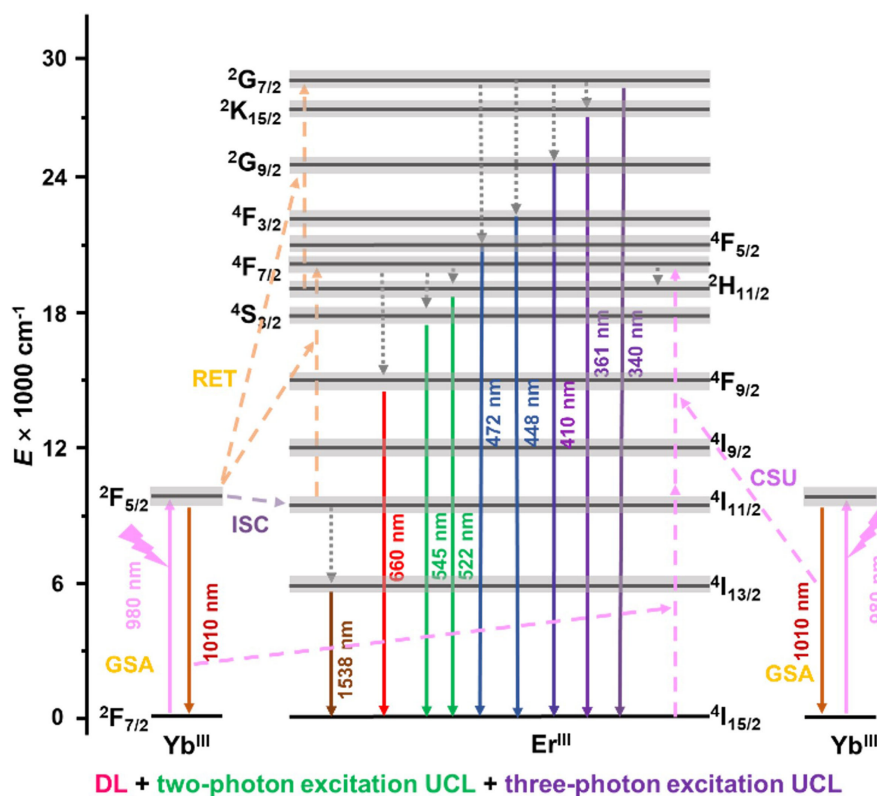


**Figure 11.** (A) Crystal structure of  $[Yb_2Er]^+$  and the positive mode of ESI-MS spectra of  $[Yb_2Er]^+/[Er_2Yb]^+$  in MeOH; (B) DL spectra ( $\lambda_{ex} = 980$  and  $400$  nm) of  $[Yb_2Er]^+$  before and after addition of 2 equiv of fluoride in solid state; (C) The fluoride-dependent UCL of  $[Yb_2Er]^+$  ( $2 \times 10^{-4}$  M) under  $2$  W/cm $^2$  in  $CH_2Cl_2$ ; (D) The P-dependent UCL of  $[Yb_2Er]^+$  ( $2 \times 10^{-4}$  M) with 3.5 molar equivalent  $[Bu_4N]F$ . This figure is used with permission from Wiley-VCH GmbH<sup>[45]</sup>. UCL: Upconversion luminescence; ESI-MS: electrospray ion mass spectra; DL: downshifting luminescence.

With the help of diamagnetic  $La^{3+}$ , the predictable hydrogen nuclear magnetic resonance ( $^1H$ NMR) spectra of  $Eu^{III}$ , and Density functional theory (DFT) calculations, scrambling possibility of different  $Ln^{III}$  in the structure could be excluded. As only the cationic motif is emissive, by merely exchanging the precursors,  $[Yb_2Er]^+$  and  $[Er_2Yb]^+$  were afforded with different ratios of S to A. Doublet emission bands from both  $Yb^{III}$  (1,010 nm) and  $Er^{III}$  (1,535 nm) were observed in both solid state [Figure 11B] and  $CH_2Cl_2$  solution at ambient atmosphere by irradiation within the absorption bands of  $Yb^{III}$  (980 nm) and Hmq/hfac $^-$  ( $250$  nm  $<$   $\lambda_{ex}$   $<$   $420$  nm). Due to strong nonradiative competitors exhausting excited energies, the hoped-for UCL could not appear. However, after introduction of 1.5 molar equivalent  $[Bu_4N]F$  into the solutions, a competitive UCL by a 980 nm laser irradiation, even with  $P = 0.288$  W/cm $^2$ , was observed, and 7.3-time emission enhancement with the optimized 3.5 molar equivalent  $[Bu_4N]F$  was present [Figure 11C]. Correspondingly, powder X-ray diffraction (PXRD), multistage mass spectra (MS), and the  $^1H$  NMR of  $[Eu_2La][La]$  were employed to confirm the stability of  $[Yb_2Er]^+$  under fluoride intervention. Since the enhancement of DL was negligible with respect to that of UCL, it is practicable to switch on UCL by fluoride association. Moreover, the competition between linear decay and UC on depletion of intermediate excited states is more intense under fluoride introduction [Scheme 1], and  $\eta_{DL}$  (0.30) was slightly higher than  $\eta_{UC}$  (0.28).



**Scheme 1.** Yb<sub>2</sub>Er-centered energy-level diagrams derived from the observed emissions associated with 3.5 equiv of fluoride and possible mechanisms highlighted. This figure is used with permission from Wiley-VCH GmbH<sup>[45]</sup>. DL: Downshifting luminescence; UCL: upconversion luminescence.

By increasing  $P$  amplifies the competition between DL and UCL [Scheme 1], the slope lower to 1.25, suggesting a saturated intermediate state. Moreover, the long risetimes, non- $P$ -dependent UCL ( $P > 2 \text{ W/cm}^2$ ), and matched energy of two sensitizers for one activator suggested both ETU and CSU mechanisms operative in  $[\text{Yb}_2\text{Er}]^+$  [Scheme 1]. Beneficial from more sensitizers energizing fewer activators within short distances (3.7 Å),  $[\text{Yb}_2\text{Er}]^+$  exhibited higher  $\Phi_{\text{UC}}$  and longer decays than  $[\text{Er}_2\text{Yb}]^+$ . More importantly, its relative  $\Phi_{\text{UC}}$  is at least twenty times stronger than that in the previous results.

As discussed above, strategies for optimizing lanthanide luminescence include making use of vibrational modes for walkable dual emissions and rotational modes for AIPE-active lanthanide complexes, even triggering the ACQ/AIE for consistent lanthanide emission, and using fluoride to prevent nonradiative processes triggering enhanced DL and even achieving high  $\Phi_{\text{UC}}$  of lanthanide complexes in solutions [Table 2]. All these strategies are based on modulation of energy levels between the photosensitizer in external simulations and the inner Ln<sup>III</sup>, corresponding to their various energy transfer rates and efficiencies. The changes of luminescence performance of lanthanide complexes smartly reflect their peripheral environment.

## VARIOUS APPLICATIONS

### Water-soluble and luminescent tracking lanthanide-complexed motors

Beneficial from noninvasive controls, light-driven molecular motors are promising for smart materials, even in bionanotechnology<sup>[47]</sup>. However, due to stilbene core structure, they are inherently hydrophobic<sup>[48]</sup>.

Although it has been demonstrated that metal-complexed motors disturb the photochemical isomerization of free motors under visible light and even experience triplet energy transfer proceeds<sup>[49,50]</sup>, most of them retain their performances in nonpolar solvents rather than aqueous mediums<sup>[51,52]</sup>. Moreover, the rotary speed in thermal helix inversion (THI) steps remains unclear, dependent on the efficiency of triplet energy transfer.

In the reaction of molecular motors based on overcrowded alkenes ( $L_m$ ) with  $Ln(NO_3)_3$ , Li *et al.* reported the first water-soluble ionic lanthanide-complexed motors  $[(L_m)_2-Ln(NO_3)_2(H_2O)_2] \cdot NO_3$  ( $Ln(L_m)_2$ )<sup>[53]</sup>. In the crystal packing [Figure 12A],  $LnL_m(R)_2$  and  $LnL_m(S)_2$  alternate stacking with each other, inducing almost no signals of the circular dichroism (CD) signals in methanol. Confirmed by only one set of <sup>1</sup>HNMR signals of  $-CH_3$ , the possible conformer of  $LnL_m(R)L_m(S)$  in solutions could be reasonably excluded. As shown in the crystal structure, the  $Ln-L_m$  interactions not only shorten  $N_1-N_2$  distances but also planarize the rotator, promoting charge transfer from ligand to metal (<sup>3</sup>LMCT). Moreover, in comparison with the decay lifetimes of phosphorescence at 530 nm of  $L_m$ , the residual ones in  $Ln(L_m)_2$  ( $Ln = Eu, Ho, Er$ ) are obviously shorter than that in  $La(L_m)_2$  by irradiation within <sup>3</sup>LMCT absorption bands, sensitizing typical lanthanide-based luminescence. Thus, by employing  $L_m$  as a sensitizer, it was able to variously induce different triplet  $\eta_{L \rightarrow Ln}$  by replacing  $Ln^{III}$  ( $Ln = Eu, Ho, Er$ ), correspondingly decreasing the intensity of low-energy <sup>3</sup>LMCT absorption in the order:  $Eu(L_m)_2 < Er(L_m)_2 < Ho(L_m)_2 < La(L_m)_2$ . Furthermore, the <sup>3</sup>LMCT sensitization of  $Eu^{III}$ -based emission of  $Eu(L_m)_2$  [Figure 12B] favors tracing its movement by delayed emission spectra [Figure 12C], and the temperature-dependent luminescence makes it as possible as luminescent thermometers.

Since the  $Ln-L_m$  interactions contract the stator to decrease the steric hindrance on the “fjord region”, accelerating the rotation of  $L_m$ <sup>[54]</sup>. From the crystal structure, “lanthanide contraction effect”, and DFT calculation [Figure 12D], the rotation followed the order:  $Er(L_m)_2 > Eu(L_m)_2 > La(L_m)_2$ . Since the heavy atom effect induced by the introduced  $Ln^{III}$  favors the percentage of triplet states of  $L_m$ <sup>[55]</sup>, and the excited state of  $Ln$ -complexed  $L_m$  is easily quenched by intramolecular rotations, the higher  $\eta_{L \rightarrow Ln}$  for triplet states, the lower energy barrier ( $\Delta^+G$ ). We thus conclude that both allostery and <sup>3</sup>LMCT sensitization cooperatively modulate their rotations as:  $La(L_m)_2 < Ho(L_m)_2 < Eu(L_m)_2 < Er(L_m)_2$ . On the other hand, hydrogen bonds around  $Ln^{III}$  favor their rotations in different aqueous mediums, inducing the rotary speed in methanol to be slower than that in water [Figure 12E]. Besides solvent effects<sup>[56]</sup>, hydrogen bonds surrounding  $Ln$ -subunits in water more and stronger than those in methanol may account for the faster rotations in  $H_2O$  than those in  $MeOH$ , favoring the THI process [Figure 12F]<sup>[57]</sup>. Therefore, this work puts up a novel strategy for water-soluble, visible-light-driven, controllable rotation, and luminescence tracing lanthanide functionalized ionic motors in an aqueous medium, pushing forward the progress of their principles and applications in biological fields.

### pH-responsive delivery and dual-modal imaging of Gd/Tm-MOFs

Beneficial from linear luminescence, large specific surface areas, and porous structures,  $Ln$ -MOFs have been widely applied to catalysis<sup>[58]</sup>, bioimaging<sup>[59]</sup>, besides sensing<sup>[60]</sup>. Due to minimal auto-fluorescence interference, deeper NIR light penetration, and slight photo-damage,  $Ln$ -MOFs with UCL offer huge potential for vivo optical imaging and bioassay<sup>[61]</sup>. It has been demonstrated that  $Gd^{3+}/Tm^{3+}$  co-doped metal-organic frameworks (MOFs) possess superior UCL and can even potentially be used as UCL/magnetic resonance image (MRI) dual-mode imaging. Herein, through a facile one-step hydrothermal method, we designed  $Gd/Tm$ -MOFs ( $[(Tm, Gd)(BTC) \cdot (H_2O) \cdot DMF]$ )<sup>[62]</sup>, which exhibited strong UCL with the lifetime of  $379 \pm 2 \mu s$  and the quantum yield of 0.76 % under the  $Tm^{3+}$  content at 6%, along with superior positive MRI. Further employing uniform mesoporous silica ( $mSiO_2$ ) shells and folic acid (FA) to functionalize

**Table 2. Differences between these three modes in discrete lanthanide complexes**

	Vibrational mode	Rotational mode	Trigger mode
Sensitizer	Conjugate aromatic sensitizer in square structure	AIE-active sensitizer	Containing nonradiative competitor
Mechanism	$\pi$ - $\pi$ stacking interactions red-shifting and shielding the fixed lanthanide emission	The enhanced excited energy of sensitizer by structural rigidification energizing the inert Ln <sup>III</sup> excited state through the antenna effect	Preventing nonradiative processes by hydrogen bonding

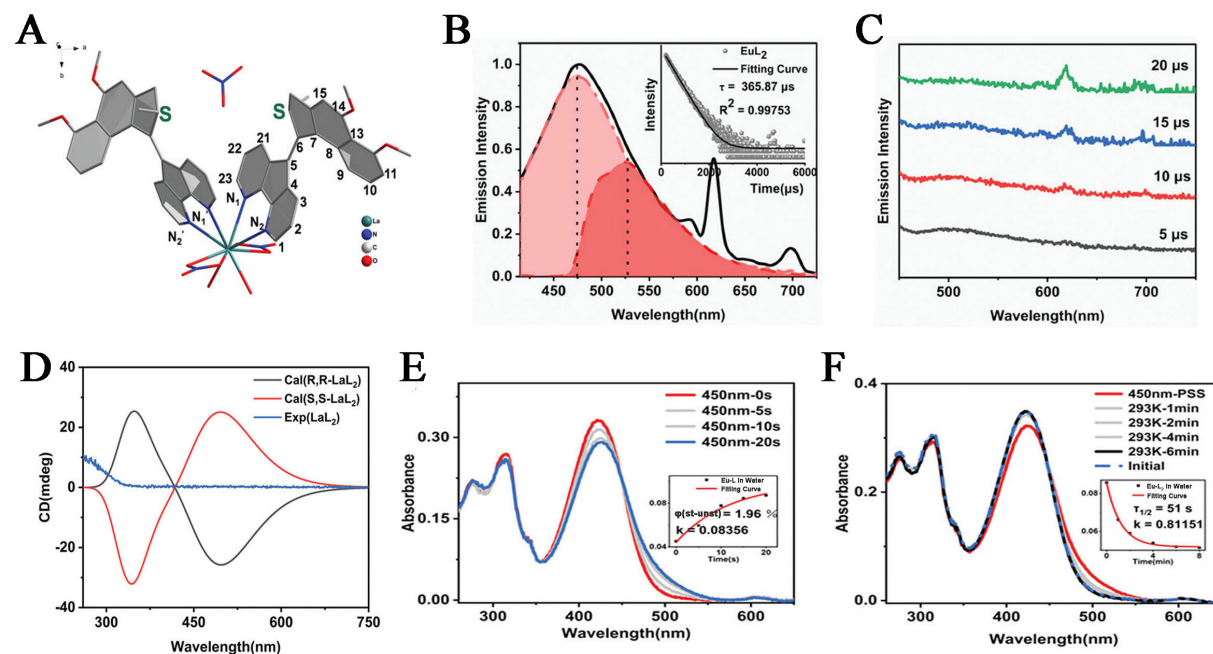


**Figure 12.** (A) Crystal structure of  $\text{La}(\text{L}_m)_2$ ; (B) emission spectra of  $\text{Eu}(\text{L}_m)_2$  and Eu-based lifetimes ( $\lambda_{em} = 616 \text{ nm}$ , inset); (C) delayed emission spectra of  $\text{Eu}(\text{L}_m)_2$  in MeOH; (D) CD spectra of  $\text{La}(\text{L}_m)_2$  [ $\text{La}(\text{L}_m)(\text{S})_2$ , black,  $\text{La}(\text{L}_m)(\text{R})_2$  red; calculated one, blue]; photochemistry (E) and THI processes (F) of  $\text{Eu}(\text{L}_m)_2$  in water. This figure is used with permission from Wiley-VCH GmbH<sup>[53]</sup>. CD: Circular dichroism; THI: thermal helix inversion.

Gd/Tm-MOFs enabled its drug loading of doxorubicin hydrochloride (DOX) from 10.6 up to 41.5 mg/g. Correspondingly, the drug release was also climbed up from 12% to 64% by precise regulation of the pH from 7.4 from 5.8 [Figure 13].

Both  $\text{Tm}^{3+}$  and  $\text{Gd}^{3+}$  in the crystal structure of Gd/Tm-MOFs exhibited a seven-coordination mode, which facilitated further interactions between the empty orbitals of  $\text{Gd}^{3+}$  and  $\text{H}_2\text{O}$  and also provided more opportunities for large positive magnetic susceptibility anisotropy of  $\text{Tm}^{3+}$  to combine with  $\text{H}_2\text{O}$  or  $-\text{OH}$  on the surface of  $\text{mSiO}_2$  shells. All these facts improved the longitudinal relativity ( $r_1$ ) value of 225.86  $\text{mM}^{-1}\cdot\text{s}^{-1}$  up to the second rank among the reported gadolinium complexes. Consequently, Gd/Tm-MOFs@ $\text{mSiO}_2$ -FA was considered as one of the promising drug carriers/releases and enabled UCL/MRI dual-mode imaging, advancing the development of accurate cancer treatment in the near future.

### Temperature sensing

In lanthanide complexes, the presence of organic chromophores allows nonradiative excited energy dissipation through molecular vibrations. Decreasing the measurement temperature prevents nonradiative energy dissipation, increasing the luminescent intensity and lifetime. Thus, studying the correlation between

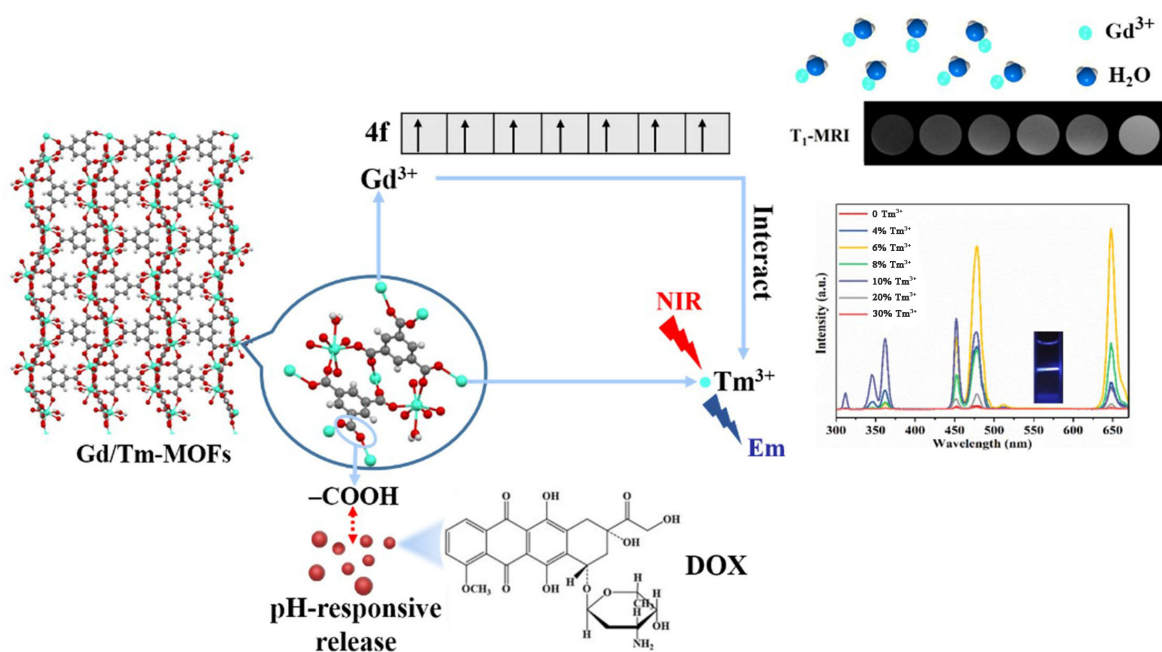


**Figure 13.** The schematic diagram of Gd/Tm-MOFs@mSiO<sub>2</sub>-FA on anti-tumor drug loading and UCL/MRI dual-mode imaging. This figure is used with permission from the Royal Society of Chemistry<sup>[62]</sup>. UCL: Upconversion luminescence; MRI: magnetic resonance image.

luminescent intensity and temperature enables the development of temperature sensors<sup>[63]</sup>. To develop non-contact thermometers with superior sensitivity and an adjustable response range, optimizing energy transfer efficiency between different energy-matched Ln<sup>III</sup> by altering their molar ratios is more practicable<sup>[64]</sup>. Recently, an easy-to-use luminescent thermometry by coating lanthanide complexes onto surfaces with an airbrush was developed<sup>[65]</sup>. By optimizing the film compositions of Tb<sup>3+</sup> and Eu<sup>3+</sup> complexes, a thermometric parameter based on the intensity ratio of green and red channels by UV-excitation was afforded, which exhibited high sensitivity (1.7%-3.6% K<sup>-1</sup>) in the 278-312 K range, making it a practical for real-time thermal monitoring of surfaces. For more information, please refer to<sup>[66,67]</sup>.

### Biological imaging

Not only responding to diverse environmental stimuli by structural modulation based on a molecular platform but also superior NIR emission, stability, and longer lifetimes enable lanthanide-coordinated compounds ideal for fluorescence lifetime imaging (FLIM)<sup>[68,69]</sup>. Highly stable and luminescent  $\beta$ -fluorinated Yb<sup>3+</sup> complexes, which exhibited strong NIR luminescence ( $\Phi = 23\%$ ) and extended decay lifetimes (249  $\mu$ s), were suitable for both steady-state and time-resolved FLIM within the NIR range<sup>[70]</sup>. Interestingly, these complexes showed specific luminescent signals, precisely revealing intracellular lifetime distributions (100-200  $\mu$ s) as FLIM. These results highlighted the potential of these NIR lanthanide complexes as efficient tools for biological imaging, offering high sensitivity and discrimination capabilities. Further to realize targeted bioimaging, a reactive chemical group, which allowed coupling to biological vectors, was employed to enhance the functionality of lanthanide luminescent bioprobes (LLBs)<sup>[71]</sup>. For instance, incorporating a primary amine on the *para*-position of the macrocyclic pyridine unit as LLBs involved them coupling to biological vectors (proteins, peptides, antibodies) for deep targeted *in vivo* bioimaging.

### Organic light-emitting diode

Lanthanide complexes with organic ligands also show great potential for applications in optoelectronic devices, particularly in organic light-emitting diodes (OLEDs)<sup>[72]</sup>. A novel class of Eu<sup>II</sup> complexes relying on



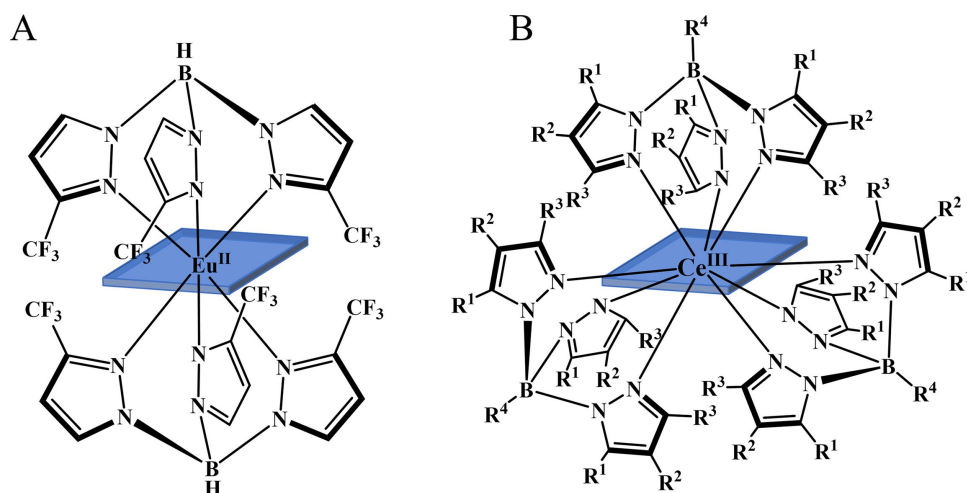


**Figure 14.** (A) Eu(II) complexes; (B) Ce(III) complexes,  $R^1 = R^3 = \text{H}$  or Me;  $R^2 = \text{H}$ , Me, Br;  $R^4 = \text{Pz}$ ,  $^n\text{Bu}$ ,  $^i\text{Pr}$ , H. The figure (A) is used with permission from the American Chemical Society<sup>[73]</sup>. The figure (B) is used with permission from Wiley-VCH GmbH<sup>[74]</sup>.

d-f transitions demonstrate high photoluminescence quantum yield (PLQY) and remarkable stability in ambient air conditions [Figure 14A]<sup>[73]</sup>. They were capable of achieving 100% exciton utilization efficiency and mitigating efficiency roll-off in OLEDs. To afford blue OLEDs, triazolyl borate with controllable substituents on the ligands of Ce(III) complexes with PLQYs > 95% for the blue 5d-4f transitions in both solid powder and diluted dichloromethane solutions and lifetimes in tens of nanoseconds range were afforded as emitting layer material [Figure 14B]<sup>[74]</sup>, achieving a maximum external quantum efficiency of 14.1% and a maximum luminance of 33,160  $\text{cd}\cdot\text{m}^{-2}$  for the blue OLEDs. These relative findings underscored the potential of lanthanide complexes in OLED applications. For more information, please refer to<sup>[72]</sup>.

## CONCLUSION AND OUTLOOK

Unlike the intermolecular energy transfer from the sensitizers to the activators controlled by second-order kinetic rate laws in lanthanide-doped solids, the one in discrete lanthanide complexes is operative by first-order kinetic rate laws. Therefore, their luminescence performance is highly dependent on that of photosensitizers, the excited energies of which are sensitive to external stimuli, inducing versatile luminescence performance of lanthanide complexes smartly reflecting the peripheral environment. Thus, multifunctional lanthanide-based hybrid luminescent materials exhibit wide applications<sup>[75]</sup>. Moreover, smart lanthanide complexes with versatile emission behaviors possessing greater superiority than traditional materials can be developed as the next generation of intelligent materials. For example, (1) different luminescence behaviors under various external stimuli are more intelligent than those of conventional functional materials that simply repeat a single behavior<sup>[76]</sup>; (2) The smart bio-probes triggered by concentrations promote consistent luminescence signals in a wide range of concentrations, not only overcoming the false detection of the traditional probe but also red-shifting the excitation wavelength to the visible region, reducing the damage to biological organisms<sup>[77]</sup>; (3) Beneficial from UV to NIR emission spectra, lanthanide-based materials usually act as both downshifting and UC layers, converting the solar spectra via luminescence to match the absorption of semiconductor devices, to improve the efficiency of solar cells<sup>[78]</sup> and so on.

Furthermore, benefiting from easy reproducibility, optical rationalization, and controlled speciation, molecular UCL, especially one of water-soluble discrete heteropolynuclear lanthanide assemblies,

potentially brings new dimensional applications, especially in deep-seated lymphoma diagnosis and optogenetics therapy. Although great progress has been made on UCL of lanthanide complexes in solution, the achievement of a high  $\Phi_{UC}$  molecular UC system under mild conditions by shifting the excitation window, regulating the excited photon transition pathway, and even in an aqueous solution suitable for bio-imaging and therapy is still on the way<sup>[79]</sup>. Thus, setting up a library of structure-property relations for functional lanthanide materials to bring new insights for a deeper understanding of future superior materials is necessary and urgent<sup>[80]</sup>.

## DECLARATIONS

### Authors' contributions

Prepared and corrected the manuscript: Fan W, Wang H, Huang X, Shi T, Du J, Xu HB

### Availability of data and materials

Not applicable.

### Financial support and sponsorship

This research was funded through the NSFC (22273019).

### Conflicts of interest

All authors declared that there are no conflicts of interest

### Ethical approval and consent to participate

Not applicable.

### Consent for publication

Not applicable.

### Copyright

© The Author(s) 2024.

## REFERENCES

1. Heffern MC, Matosziuk LM, Meade TJ. Lanthanide probes for bioresponsive imaging. *Chem Rev* 2014;114:4496-539. [DOI](#) [PubMed](#) [PMC](#)
2. Pershagen E, Nordholm J, Borbas KE. Luminescent lanthanide complexes with analyte-triggered antenna formation. *J Am Chem Soc* 2012;134:9832-5. [DOI](#) [PubMed](#)
3. Pei K, Wu J, Zhao M, et al. Polarized emission of lanthanide metal-organic framework (Ln-MOF) crystals for high-capacity photonic barcodes. *Adv Opt Mater* 2022;10:2102143. [DOI](#)
4. Jia T, Chen G. Lanthanide nanoparticles for near-infrared II theranostics. *Coord Chem Rev* 2022;471:214724. [DOI](#)
5. Song B, Shi W, Shi W, et al. A dual-modal nanoprobe based on Eu(III) complex-MnO<sub>2</sub> nanosheet nanocomposites for time-gated luminescence-magnetic resonance imaging of glutathione *in vitro* and *in vivo*. *Nanoscale* 2019;11:6784-93. [DOI](#)
6. Sørensen TJ, Tropiano M, Blackburn OA, Tilney JA, Kenwright AM, Faulkner S. Preparation and study of an f,f,f,f" covalently linked tetranuclear hetero-trimetallic complex - a europium, terbium, dysprosium triad. *Chem Commun* 2013;49:783-5. [DOI](#)
7. Hasegawa Y, Kitagawa Y, Nakanishi T. Effective photosensitized, electrosensitized, and mechanosensitized luminescence of lanthanide complexes. *NPG Asia Mater* 2018;10:52-70. [DOI](#)
8. Binnemans K. Lanthanide-based luminescent hybrid materials. *Chem Rev* 2009;109:4283-374. [DOI](#) [PubMed](#)
9. D'Aléo A, Pointillart F, Ouahab L, Andraud C, Maury O. Charge transfer excited states sensitization of lanthanide emitting from the visible to the near-infrared. *Coord Chem Rev* 2012;256:1604-20. [DOI](#)
10. Xu LJ, Xu GT, Chen ZN. Recent advances in lanthanide luminescence with metal-organic chromophores as sensitizers. *Coord Chem Rev* 2014;273-4:47-62. [DOI](#)
11. Xu HB, Zhang LY, Xie ZL, Ma E, Chen ZN. Heterododecanuclear Pt<sub>6</sub>Ln<sub>6</sub> (Ln = Nd, Yb) arrays of 4-ethynyl-2,2'-bipyridine with sensitized near-IR lanthanide luminescence by Pt → Ln energy transfer. *Chem Commun* 2007:2744-6. [DOI](#) [PubMed](#)
12. Xu HB, Chen XL, Deng JG, et al. Sensitized near infrared emission through supramolecular d → f energy transfer within an ionic

- Ru(ii)-Er(iii) pair. *Dalton Trans* 2018;47:2073-8. DOI
13. Mara D, Artizzu F, Smet PF, Kaczmarek AM, Van Hecke K, Van Deun R. Vibrational quenching in near-infrared emitting lanthanide complexes: a quantitative experimental study and novel insights. *Chemistry* 2019;25:15944-56. DOI PubMed
  14. Han S, Deng R, Gu Q, et al. Lanthanide-doped inorganic nanoparticles turn molecular triplet excitons bright. *Nature* 2020;587:594-9. DOI
  15. Qin CY, Gao JH, Xie XB, Zhai CP, Li HQ, Ma Y. Crystalline phase-dependent cations migration in core-shell lanthanide-doped upconversion nanoparticles. *Chem Synth* 2023;3:29. DOI
  16. Zhu X, Su Q, Feng W, Li F. Anti-Stokes shift luminescent materials for bio-applications. *Chem Soc Rev* 2017;46:1025-39. DOI
  17. Charbonnière LJ. Bringing upconversion down to the molecular scale. *Dalton Trans* 2018;47:8566-70. DOI
  18. Hyppänen I, Lahtinen S, Ääritalo T, Mäkelä J, Kankare J, Soukka T. Photon upconversion in a molecular lanthanide complex in anhydrous solution at room temperature. *ACS Photonics* 2014;1:394-7. DOI
  19. Singh-Rachford TN, Castellano FN. Photon upconversion based on sensitized triplet-triplet annihilation. *Coord Chem Rev* 2010;254:2560-73. DOI
  20. Kiseleva N, Nazari P, Dee C, et al. Lanthanide sensitizers for large anti-stokes shift near-infrared-to-visible triplet - triplet annihilation photon upconversion. *J Phys Chem Lett* 2020;11:2477-81. DOI PubMed
  21. Kalmbach J, Wang C, You Y, et al. Near-IR to near-IR upconversion luminescence in molecular chromium ytterbium salts. *Angew Chem Int Ed Engl* 2020;59:18804-8. DOI PubMed PMC
  22. Chorazy S, Wyczęsany M, Sieklucka B. Lanthanide photoluminescence in heterometallic polycyanidometallate-based coordination networks. *Molecules* 2017;22:1902. DOI PubMed PMC
  23. Wang C, Otto S, Dorn M, et al. Deuterated molecular ruby with record luminescence quantum yield. *Angew Chem Int Ed Engl* 2018;57:1112-6. DOI
  24. Sun G, Xie Y, Wang Y, et al. Cooperative sensitization upconversion in solution dispersions of co-crystal assemblies of mononuclear Yb<sup>3+</sup> and Eu<sup>3+</sup> complexes. *Angew Chem Int Ed Engl* 2023;62:e202304591. DOI PubMed
  25. Punj D, Mivelle M, Moparthi SB, et al. A plasmonic “antenna-in-box” platform for enhanced single-molecule analysis at micromolar concentrations. *Nat Nanotechnol* 2013;8:512-6. DOI PubMed
  26. Xu HB, Zhang LY, Ni J, Chao HY, Chen ZN. Conformation changes and luminescent properties of Au-Ln (Ln = Nd, Eu, Er, Yb) arrays with 5-ethynyl-2,2'-bipyridine. *Inorg Chem* 2008;47:10744-52. DOI PubMed
  27. Xu HB, Deng JG, Kang B. Designed synthesis and photophysical properties of multifunctional hybrid lanthanide complexes. *RSC Adv* 2013;3:11367-84. DOI
  28. Xu HB, Wang J, Chen XL, et al. Regulating structural dimensionality and emission colors by organic conjugation between Sm<sup>III</sup> at a fixed distance. *Dalton Trans* 2018;47:6908-16. DOI
  29. Gállico DA, Ovens JS, Sigoli FA, Murugesu M. Room-temperature upconversion in a nanosized {Ln<sub>15</sub>} molecular cluster-aggregate. *ACS Nano* 2021;15:5580-5. DOI PubMed
  30. Xu HB, Jiao PC, Kang B, Deng JG, Zhang Y. Walkable dual emissions. *Sci Rep* 2013;3:2199. DOI PubMed PMC
  31. Huang K, Wu H, Shi M, Li F, Yi T, Huang C. Reply to comment on “aggregation-induced phosphorescent emission (AIPE) of iridium(iii) complexes”: origin of the enhanced phosphorescence. *Chem Commun* 2009:1243-5. DOI
  32. Hong Y, Lam JWY, Tang BZ. Aggregation-induced emission: phenomenon, mechanism and applications. *Chem Commun* 2009:4332-53. DOI
  33. Martinić I, Eliseeva SV, Nguyen TN, Pecoraro VL, Petoud S. Near-infrared optical imaging of necrotic cells by photostable lanthanide-based metallacrowns. *J Am Chem Soc* 2017;139:8388-91. DOI PubMed
  34. Zhuo H, Guan DB, He JC, Xu HB, Zeng MH. Stepwise increase of Nd<sup>III</sup>-based phosphorescence by AIE-active sensitizer: broadening the AIPE family from transition metals to discrete near-infrared lanthanide complexes<sup>\*</sup>. *Chemistry* 2021;27:16204-11. DOI PubMed
  35. Tinnefeld P. Single-molecule detection: Breaking the concentration barrier. *Nat Nanotechnol* 2013;8:480-2. DOI PubMed
  36. Zhang Y, Jiao PC, Xu HB, et al. Switchable sensitizers stepwise lighting up lanthanide emissions. *Sci Rep* 2015;5:9335. DOI PubMed PMC
  37. Alric C, Taleb J, Le Duc G, et al. Gadolinium chelate coated gold nanoparticles as contrast agents for both X-ray computed tomography and magnetic resonance imaging. *J Am Chem Soc* 2008;130:5908-15. DOI
  38. Lewis DJ, Glover PB, Solomons MC, Pikramenou Z. Purely heterometallic lanthanide(III) macrocycles through controlled assembly of disulfide bonds for dual color emission. *J Am Chem Soc* 2011;133:1033-43. DOI PubMed
  39. Xu HB, Deng JG, Zhang LY, Chen ZN. Structural and photophysical studies on geometric (Er<sub>2</sub>Yb<sub>2</sub>/Yb<sub>2</sub>Er<sub>2</sub>) and configurational (EuTb<sub>3</sub>/Eu<sub>3</sub>Tb) isomers of heterotetranuclear lanthanide(III) complexes. *Cryst Growth Des* 2013;13:849-57. DOI
  40. Knighton RC, Soro LK, Lecointre A, et al. Upconversion in molecular hetero-nonanuclear lanthanide complexes in solution. *Chem Commun* 2021;57:53-6. DOI
  41. Golesorkhi B, Fürstenberg A, Nozary H, Piguet C. Deciphering and quantifying linear light upconversion in molecular erbium complexes. *Chem Sci* 2019;10:6876-85. DOI PubMed PMC
  42. Kalmbach J, Wang C, You Y, et al. NIR-NIR-Aufkonvertierung in molekularen Chrom-Ytterbium-Salzen. *Angew Chem Int Ed* 2020;132:18966-70. DOI
  43. Mo JT, Wang Z, Fu PY, et al. Highly efficient DCL, UCL, and TPEF in hybridized Ln-complexes from Ir-metalloligand. *CCS Chem* 2021;3:729-38. DOI

44. Aboshyan-Sorgho L, Besnard C, Pattison P, et al. Near-infrared→visible light upconversion in a molecular trinuclear d-f-d complex. *Angew Chem Int Ed Engl* 2011;50:4108-12. DOI PubMed
45. Wang J, Jiang Y, Liu JY, et al. Discrete heteropolynuclear Yb/Er assemblies: switching on molecular upconversion under mild conditions. *Angew Chem Int Ed Engl* 2021;60:22368-75. DOI
46. Xu HB, Zhong YT, Zhang WX, Chen ZN, Chen XM. Syntheses, structures and photophysical properties of heterotrinuclear Zn<sub>2</sub>Ln clusters (Ln = Nd, Eu, Tb, Er, Yb). *Dalton Trans* 2010;39:5676-82. DOI PubMed
47. Wang J, Feringa BL. Dynamic control of chiral space in a catalytic asymmetric reaction using a molecular motor. *Science* 2011;331:1429-32. DOI
48. Pooler DRS, Lubbe AS, Crespi S, Feringa BL. Designing light-driven rotary molecular motors. *Chem Sci* 2021;12:14964-86. DOI PubMed PMC
49. Kassem S, van Leeuwen T, Lubbe AS, Wilson MR, Feringa BL, Leigh DA. Artificial molecular motors. *Chem Soc Rev* 2017;46:2592-621. DOI PubMed
50. Wezenberg SJ, Chen KY, Feringa BL. Visible-light-driven photoisomerization and increased rotation speed of a molecular motor acting as a ligand in a ruthenium(II) complex. *Angew Chem Int Ed Engl* 2015;54:11457-61. DOI
51. Faulkner A, van Leeuwen T, Feringa BL, Wezenberg SJ. Allosteric regulation of the rotational speed in a light-driven molecular motor. *J Am Chem Soc* 2016;138:13597-603. DOI PubMed PMC
52. Cnossen A, Hou L, Pollard MM, Wesenhagen PV, Browne WR, Feringa BL. Driving unidirectional molecular rotary motors with visible light by intra- and intermolecular energy transfer from palladium porphyrin. *J Am Chem Soc* 2012;134:17613-9. DOI PubMed
53. Li S, Zhao Y, Li Q, Li M, Zhang X, Xu HB. Lanthanide-functionalized water-soluble ionic motors: synergetically regulated rotary motion by allostery and triplet sensitization. *Adv Opt Mater* 2023;11:2300179. DOI
54. Iino R, Kinbara K, Bryant Z. Introduction: molecular motors. *Chem Rev* 2020;120:1-4. DOI PubMed
55. Eliseeva SV, Bünzli JCG. Lanthanide luminescence for functional materials and bio-sciences. *Chem Soc Rev* 2010;39:189-227. DOI PubMed
56. Lubbe AS, Kistemaker JCM, Smits EJ, Feringa BL. Solvent effects on the thermal isomerization of a rotary molecular motor. *Phys Chem Chem Phys* 2016;18:26725-35. DOI PubMed
57. Wiedbrauk S, Maerz B, Samoylova E, et al. Twisted hemithioindigo photoswitches: solvent polarity determines the type of light-induced rotations. *J Am Chem Soc* 2016;138:12219-27. DOI
58. Dasari S, Singh S, Sivakumar S, Patra AK. Dual-sensitized luminescent europium(III) and terbium(III) complexes as bioimaging and light-responsive therapeutic agents. *Chemistry* 2016;22:17387-96. DOI PubMed
59. Weng H, Yan B. A flexible Tb(III) functionalized cadmium metal organic framework as fluorescent probe for highly selectively sensing ions and organic small molecules. *Sens Actuators B Chem* 2016;228:702-8. DOI
60. Wang X, Jiang Y, Tissot A, Serre C. Luminescent sensing platforms based on lanthanide metal-organic frameworks: current strategies and perspectives. *Coord Chem Rev* 2023;497:215454. DOI
61. Lin M, Gao Y, Hornicek F, et al. Near-infrared light activated delivery platform for cancer therapy. *Adv Colloid Interface Sci* 2015;226:123-37. DOI PubMed PMC
62. Liu Y, Zhang C, Xu C, et al. Controlled synthesis of up-conversion luminescent Gd/Tm-MOFs for pH-responsive drug delivery and UCL/MRI dual-modal imaging. *Dalton Trans* 2018;47:11253-63. DOI
63. Kenney JW, Lee JJ. Photoluminescent metal complexes and materials as temperature sensors - an introductory review. *Chemosensors* 2021;9:109. DOI
64. Brites CDS, Balabhadra S, Carlos LD. Lanthanide-based thermometers: at the cutting-edge of luminescence thermometry. *Adv Opt Mater* 2019;7:1801239. DOI
65. Marin R, Millan NC, Kelly L, et al. Luminescence thermometry using sprayed films of metal complexes. *J Mater Chem C* 2022;10:1767-75. DOI
66. Vanden Bussche F, Kaczmarek AM, Van Speybroeck V, Van Der Voort P, Stevens CV. Overview of N-rich antennae investigated in lanthanide-based temperature sensing. *Chemistry* 2021;27:7214-30. DOI PubMed
67. Zairov RR, Dovzhenko AP, Podyachev SN, et al. Role of PSS-based assemblies in stabilization of Eu and Sm luminescent complexes and their thermoresponsive luminescence. *Colloids Surf B Biointerfaces* 2022;217:112664. DOI
68. Peng XX, Zhu XF, Zhang JL. Near infrared (NIR) imaging: exploring biologically relevant chemical space for lanthanide complexes. *J Inorg Biochem* 2020;209:111118. DOI PubMed
69. Zairov RR, Dovzhenko AP, Sapunova AS, et al. Dual red-NIR luminescent Eu-Yb heterolanthanide nanoparticles as promising basis for cellular imaging and sensing. *Mater Sci Eng C Mater Biol Appl* 2019;105:110057. DOI PubMed
70. Ning Y, Tang J, Liu YW, Jing J, Sun Y, Zhang JL. Highly luminescent, biocompatible ytterbium(III) complexes as near-infrared fluorophores for living cell imaging. *Chem Sci* 2018;9:3742-53. DOI PubMed PMC
71. Hamon N, Bridou L, Roux M, Maury O, Tripier R, Beyler M. Design of bifunctional pycnol-based lanthanide luminescent bioprobes for targeted two-photon imaging. *J Org Chem* 2023;88:8286-99. DOI PubMed
72. Wang L, Zhao Z, Wei C, et al. Review on the electroluminescence study of lanthanide complexes. *Adv Opt Mater* 2019;7:1801256. DOI
73. Zhan G, Wang L, Zhao Z, Fang P, Bian Z, Liu Z. Highly efficient and air-stable lanthanide Eu<sup>III</sup> complex: new emitter in organic light emitting diodes. *Angew Chem Int Ed Engl* 2020;59:19011-5. DOI PubMed

74. Fang P, Wang L, Zhan G, et al. Lanthanide cerium(III) tris(pyrazolyl)borate complexes: efficient blue emitters for doublet organic light-emitting diodes. *ACS Appl Mater Interfaces* 2021;13:45686-95. DOI PubMed
75. Zairov RR, Dovzhenko AP, Sapunova AS, et al. Terbium(III)-thiacalix[4]arene nanosensor for highly sensitive intracellular monitoring of temperature changes within the 303-313 K range. *Sci Rep* 2020;10:20541. DOI PubMed PMC
76. Wang Y, Li H, He X, Xu Z. Application in anticounterfeiting for multistimuli smart luminescent materials based on MOF-on-MOF. *Inorg Chem* 2021;60:15001-9. DOI
77. Guo WJ, Peng T, Zhu W, et al. Visualization of supramolecular assembly by aggregation-induced emission. *Aggregate* 2023;4:e297. DOI
78. Zheng B, Fan J, Chen B, et al. Rare-earth doping in nanostructured inorganic materials. *Chem Rev* 2022;122:5519-603. DOI
79. Bolvin H, Fürstenberg A, Golesorkhi B, Nozary H, Taarit I, Piguet C. Metal-based linear light upconversion implemented in molecular complexes: challenges and perspectives. *Acc Chem Res* 2022;55:442-56. DOI PubMed
80. Huang Q, Zhang Y, She S, Fan W, Hou C, Xu HB. Lanthanide composite as doping reagent simplifies and uniformizes deposition of fiber preforms. *Cell Rep Phys Sci* 2023;4:101716. DOI